HHS Public Access

Author manuscript

Mol Cell. Author manuscript; available in PMC 2016 February 05.

Published in final edited form as:

Mol Cell. 2015 February 5; 57(3): 479–491. doi:10.1016/j.molcel.2014.12.018.

Interdependence of the Rad50 hook and globular domain functions

Marcel Hohl[1], **Tomasz Kochańczyk**[2], **Cristina Tous**[3], **Andrés Aguilera**[3], **Artur Krężel**[2], and **John H J Petrini**[1]

[1]Molecular Biology Program, Memorial Sloan-Kettering Cancer Center, New York, NY 10021, USA [2]Laboratory of Chemical Biology, University of Wrocław, Joliot-Curie 14a, 50-383 Wrocław, Poland [3]Centro Andaluz de Biología Molecular y Medicina Regenerativa CABIMER, Universidad de Sevilla, Avenida Américo Vespucio s/n, 41092 Sevilla, Spain

SUMMARY

Rad50 contains a conserved Zn^{2+} coordination domain (the Rad50 hook) that functions as a homodimerization interface. Hook ablation phenocopies Rad50 deficiency in all respects. Here we focused on *rad50* mutations flanking the Zn^{2+}-coordinating hook cysteines. These mutants impaired hook-mediated dimerization, but recombination between sister chromatids was largely unaffected. This may reflect that cohesin-mediated sister chromatid interactions are sufficient for double strand break repair. However, Mre11 complex functions specified by the globular domain, including Tel1 (ATM) activation, nonhomologous end-joining, and DNA double strand break end resection were affected, suggesting that dimerization exerts a broad influence on Mre11 complex function. These phenotypes were suppressed by mutations within the coiled coil and globular ATPase domain, suggesting a model in which conformational changes in the hook and globular domains are transmitted via the extended coils of Rad50. We propose that transmission of spatial information in this manner underlies the regulation of Mre11 complex functions.

Keywords

DNA repair; Rad50; Mre11 complex; hook; double strand break; coiled coil

INTRODUCTION

The Mre11 complex is an oligomeric assembly comprising dimers of Mre11, Rad50, and Xrs2 in budding yeast (or Nbs1 in fission yeast and other eukaryotes). The Mre11 complex

*Corresponding author: John H. J. Petrini, Memorial Sloan-Kettering Cancer Center, 1275 York Avenue, New York, NY 10021. Phone: 212-639-2927, Fax: 646-422-2062, petrinij@mskcc.org.

AUTHOR CONTRIBUTIONS

MH, TK and CT performed experiments and analyzed the data. JHJP designed research in consultation with AA and AK. JHJP and MH wrote the manuscript.

exerts a broad influence on the DNA damage response (DDR) network, first as a sensor of DNA double strand breaks (DSBs), and subsequently as a mediator of DDR signaling and DSB repair. Mre11 complex-dependent DDR signaling primarily occurs via Tel1/ATM, the activation of which requires the Mre11 complex (Stracker and Petrini, 2011). Recent data also suggest a role for the Mre11 complex in the activation of ATR, the checkpoint kinase activated in response to DNA replication associated stress (Duursma et al., 2013; Shiotani et al., 2013; Stiff et al., 2004). The mechanistic basis of ATM (or ATR) activation by the Mre11 complex has not been established, although evidence that activation of ATM is influenced by Rad50-dependent ATP binding and hydrolysis is emerging (Al-Ahmadie et al., 2014; Deshpande et al., 2014; Hopfner, 2014; Lee et al., 2013). Underscoring its importance for ATM activation and signaling is the fact that mutations affecting the Mre11 complex in humans underlie cancer predisposition syndromes that exhibit phenotypic similarities to ataxia telangiectasia, a syndrome resulting from ATM deficiency (Stracker and Petrini, 2011; Stracker et al., 2013).

The Mre11 complex has an elongated structure characteristic of SMC (Structural Maintenance of Chromosomes) protein family members (de Jager et al., 2004; Wyman et al., 2011). It consists of a globular domain, from which the antiparallel coiled coil domains of each Rad50 extend, spanning approximately 500 amino acids in each direction (Stracker and Petrini, 2011). At the apex of the Rad50 coiled coil lies the Rad50 hook domain, which is characterized by two invariant cysteine residues separated by two hydrophobic amino acids (CXXC; Figure 1A). Two Rad50 hook domains can dimerize via tetrahedral coordination of a zinc ion by the two pairs of invariant cysteines; the hook domain is thus a Zn^{2+}-dependent interaction interface (Hopfner et al., 2002) (Figure 1B). Based on genetic and structural data, we have proposed that the orientation of the dimerized Rad50 coiled coil domains imposed by hook domain-mediated dimerization promotes the bridging of sister chromatids to facilitate sister chromatid recombination (SCR) (Bressan et al., 1999; Hohl et al., 2011; Hopfner et al., 2002; Moreno-Herrero et al., 2005; van der Linden et al., 2009; Wiltzius et al., 2005).

The influences of the hook and coiled coil domains appear to be largely structural, as the globular domain is the center of Mre11 complex enzymatic activities; the Mre11 nuclease domain and domains governing Rad50 ATP binding and hydrolysis reside within it (Stracker and Petrini, 2011; Williams et al., 2008; Williams and Tainer, 2005). DNA binding by the Mre11 complex also occurs within the globular domain; however a precise definition of DNA binding by the Mre11 complex is lacking, and it appears likely that more than one mode of DNA engagement by the globular domain is operative (Rojowska et al., 2014).

Recent structural studies revealed that Rad50 ATP binding and hydrolysis underlie large scale structural transitions of the Mre11 complex (Lammens et al., 2011; Lim et al., 2011; Williams et al., 2011). Upon ATP binding, Rad50 dimerizes and forms a closed complex, proposed to mediate DNA end binding, DNA end tethering, ATM checkpoint signaling and nonhomologous end-joining (NHEJ) (Deshpande et al., 2014; Lee et al., 2013). Upon ATP hydrolysis, the globular domain assumes an open configuration, promoting Mre11 nuclease activity, DNA end resection and DSB repair by homologous recombination (Deshpande et

al., 2014; Lammens et al., 2011). Although it is several hundred angstroms distal to the globular domain, the hook domain may also influence the transition from open to closed conformation (Deshpande et al., 2014; Lee et al., 2013).

Having previously shown that mutations of the invariant hook cysteines disrupt Mre11 complex integrity (Hopfner et al., 2002), we sought to establish hypomorphic mutations that impaired, but did not abolish hook domain function. We reasoned that such alleles would reveal Mre11 complex DDR activities directly dependent on the Rad50 hook domain. We randomly mutagenized the conserved hydrophobic XX-residues situated between the invariant cysteines (CXXC), as structural and biophysical data regarding the *P. furiosus* hook dimer suggested that these residues constitute a hydrophobic interface stabilizing the zinc hook dimer assembly (Hopfner et al., 2002; Kochanczyk et al., 2013). We focused on three (of over 40) alleles, designated *rad50-46*, *rad50-47*, and *rad50-48* (referred to collectively as *rad50*^{hook}; Figure 1A).

Through genetic, biochemical, and biophysical assessments, we established evidence that the *rad50*^{hook} alleles partially destabilized hook dimerization. The phenotypic outcomes were diverse, affecting myriad Mre11 complex functions, most of which appear to be specified within the globular domain. Tel1 (ATM) activation was impaired in each of the *rad50*^{hook} mutants, whereas homologous recombination, which requires hook-mediated dimerization (Hohl et al., 2011; Wiltzius et al., 2005), remained largely intact.

These *rad50*^{hook} phenotypes suggest that the stability of hook dimerization domain influences the disposition of the globular domain, and thereby functions mediated by domains within it. Mutations within the coiled coil and globular domains suppressed some of the *rad50-46* phenotypes, supporting the interpretation that the hook and globular domains of the Mre11 complex function interdependently, and that the coiled coil domains are integral to that interaction.

RESULTS

Rad50 hook alleles with partial damage sensitivity

The Rad50 hook motif consists of two invariant cysteines separated by two hydrophobic residues (CXXC); over 80% of known hook domains conform to a C(P/Y)(L/V)C consensus (Pfam database ID: PF04423). *P. furiosus* Pro445 and Val446 were shown to bind in trans to a hydrophobic groove formed at the hook loop base of the distal protomer (Hopfner et al., 2002; Kochanczyk et al., 2013). In light of their conservation, it is likely that the corresponding residues in other organisms also stabilize the zinc hook dimer assembly.

In this study, we examined the biological functions influenced by the Rad50 hook domain. Having shown that mutation of the invariant cysteines phenocopied complete Rad50 inactivation (Hopfner et al., 2002), we reasoned that mutation within these hydrophobic residues of the hook would destabilize, but not destroy the Zn^{2+}-mediated assembly, and so would confer a circumscribed effect, confined to alteration of Rad50 hook function. Random mutagenesis of the codons encoding Y688 and L689 of the *S. cerevisiae RAD50* gene was carried out, and the resulting >40 mutants were screened for MMS (methyl

methanesulfonate) sensitivity. In some instances, the primers used for mutagenesis also introduced a S to R change at position 685 (S685R). Most mutants obtained were essentially wild-type for MMS sensitivity, and two mutants phenocopied *rad50*Δ (Table S2). These two classes of mutants were not examined further. In this study we focused on the three *rad50*^{hook} alleles, *rad50-46*, *rad50-47*, and *rad50-48* (Figure 1A).

rad50-46 (S685R Y688E) and *rad50-47* (L689R) showed partial MMS, HU (hydroxyurea) and CPT *(*camptothecin) sensitivity (Figure 1C). *rad50-46* was slightly more sensitive than *rad50-47*, the later comparable to a Mre11 nuclease dead mutant *(mre11-3)*, whereas a hook cysteine mutant *(rad50-C1G)* deficient in Zn^{2+} coordination was indistinguishable from *rad50*Δ. *rad50-46* damage sensitivity was a composite effect of two mutations (S685R Y688E), as neither single mutant was sensitive (data not shown). *rad50-48* (S685R Y688R) resulted in minimal MMS sensitivity (Figure 1C). Damage survival of *rad50-46* and *rad50-47*, but not of *rad50-48*, was strongly temperature dependent, only mildly sensitive at 30°C, but highly sensitive at both 23°C and 37°C (Figure S1). As they appeared to represent hypomorphic defects in hook function, *rad50-46*, *-47*, and *-48* were retained for further analysis.

Rad50 hook mutants alter zinc hook dimerization

To determine whether the partial damage sensitivity of *rad50-46* and *rad50-47* was a result of impaired hook function, we examined the dimerization, Zn^{2+} binding and accompanying conformational changes of peptides encompassing 41 or 68 amino acids. The peptides (Table S3 and S4) included the hook domain as well as the adjacent coiled coils on either side that mediate the aforementioned intermolecular hook and coiled coil interactions. As with previous studies of the archaeal hook peptide (Kochanczyk et al., 2013), fluorescence anisotropy, circular dichroism and UV spectroscopy were employed to examine the molecular outcomes of the *rad50-46*, *-47*, and *-48* mutations (Figure 2A–C).

In the anisotropy studies, homotypic fluorescence energy transfer (homo-FRET) between 5-carboxyfluorescein moieties appended to the N-termini of the 68-mer peptides was monitored over a wide range of free Zn^{2+} concentrations. With the wild-type peptide, we observed a decrease in fluorescence anisotropy to approximately 3/4 of its initial value at subnanomolar free Zn^{2+}($-\log[Zn^{2+}] < 10$), which we interpreted as an effect of homo-FRET due to formation of Zn^{2+} induced hook dimers (Hamman et al., 1996). The *rad50-46*, *-47*, and *-48* mutants did not show appreciable Zn^{2+} dependent anisotropy, suggesting either that Zn^{2+} binding or Zn^{2+}-mediated dimerization is impaired (Figure 2A). An alternative explanation is that the geometry of the coiled coils is altered by the hook mutations, placing the 5-carboxyfluorescein moiety at a suboptimal distance for homotypic FRET to occur.

To address this issue, we used UV spectroscopy to monitor ligand to metal charge transfer (LMCT), which occurs upon Zn^{2+} coordination by cysteines (Figure 2B). In this setting LMCT is detected by UV absorbance at 222 nm. Under the conditions used, increased absorbance as a function of increasing Zn^{2+} concentration can be used to infer Zn^{2+} binding stoichiometry. In all cases we observed a linear correlation between Zn^{2+} concentration and UV absorbance over 0.0 to 0.5 (Figure 2B). For the wild-type peptide, but not *rad50-46*, *-47*, and *-48*, an inflection point was noted at the Zn^{2+}:peptide ratio of 0.5 (Figure 2B). This is

consistent with the appearance of relatively stable Zn^{2+} dependent species in which two peptides coordinate one Zn^{2+} ion. In all cases, the absorbance continues to increase over Zn^{2+}:peptide molar ratios of 0.5 to 1.0. This indicates that presumptive higher order structures are dynamic under these conditions, and at higher Zn^{2+} concentrations, individual peptides bound to Zn^{2+} predominate. The lack of a marked inflection point in the mutants argues that dimerization is somehow aberrant, possibly due to altered secondary structure of the hook domain, as suggested by the CD spectra (Figure 2C) as well as anisotropy data (Figure 2A).

Consistent with the *in vitro* data, yeast 2-hybrid analysis data suggested that zinc-dependent hook homodimerization was impaired in all *rad50^{hook}* mutants (Figure S2A–C).

Rad50 hook mutants destabilize the Rad50-Mre11 interaction

The Rad50 hook domain is critical for Mre11 complex-dependent DNA repair functions (Hohl et al., 2011; Hopfner et al., 2002; Wiltzius et al., 2005), and for the stability of the Mre11 complex (Hopfner et al., 2002). We assessed the effect of hook mutations on Mre11 complex stability by co-immunoprecipitation from whole cell extracts of *rad50-46*, *-47*, and *-48* mutants (Figure 3A). Rad50-Mre11 interaction was strongly impaired in *rad50-46*, approximating the reduction seen in *rad50-C2A* (second invariant cysteine mutated to alanine). Rad50-Mre11 interactions were reduced to a lesser extent in *rad50-47* and *rad50-48*, but were nonetheless clearly affected relative to wild-type (Figure 3A). Western blot analysis indicated that levels of the Rad50-46, -47, and -48 were unaltered. These results were confirmed by reciprocal co-immunoprecipitations (Figure S3) and by yeast 2-hybrid analysis assessing the Rad50-Mre11 interaction (data not shown). Hence, both hook dimerization and the Mre11-Rad50 interaction are destabilized in *rad50^{hook}* mutant cells.

DSB repair in hook mutants

The changes in Mre11 complex stability notwithstanding, the *rad50^{hook}* mutants did not exhibit pronounced MMS sensitivity (Figure 1C), suggesting that *rad50-46*, *-47*, and *-48* mutants were proficient in sister chromatid based homologous recombination (SCR). We used a plasmid-based SCR assay described previously to address that interpretation (Cortes-Ledesma and Aguilera, 2006; González-Barrera et al., 2003; Hohl et al., 2011). Briefly, a HO-DSB is created during S-phase and the disappearance of the 2.4 kb HO-DSB restriction fragment and appearance of a 4.7 kb SCR repair product can be monitored by Southern blotting with a *LEU2* specific probe (Figure 3B). In a time course over 9 hours, SCR products accumulated in all *rad50^{hook}* mutants to similar levels *(rad50-46*, 4.6 ± 0.7%; *rad50-47*, 5.9 ± 0.1%; *rad50-48*, 6.7 ± 1.0%), as in wild-type (6.3 ± 0.6%), albeit with slightly delayed kinetics, whereas *rad50*Δ defective in SCR showed only residual repair products (1.6 ± 0.02%; Figure 3B, quantification on right). Hence, as suggested by the MMS resistance, *rad50-46*, *-47*, and *-48* mutants are largely proficient in SCR.

The reduced SCR kinetics observed might account for its partial damage sensitivity at higher MMS doses (Figure 1C and Figure S1), and for the fact that *rad50^{hook}* mutations were associated with a mild hyper recombination phenotype. Spontaneous heteroallelic recombination between the *ade2* heteroalleles, *ade2-n* and *ade2-ISceI*, (Huang and

Symington, 1994), evident as white *ADE2* sectors within an otherwise red *ade2* colony, was only mildly increased in *rad50*^{hook} mutants. *rad50*Δ showed an average of >10 sectors per colony and sectoring decreased from *rad50-46* (5.7 ± 0.2), to *rad50-47* (3.9 ± 0.5) to wild-type levels (1.3 ± 0.4) in *rad50-48* (1.1 ± 0.1) (Figure 3C).

We showed previously that truncation of the coiled coil domain exerted a similarly mild effect on SCR. In that setting, we observed a strong defect in NHEJ, leading us to propose a model wherein structural alterations within the coiled coils would lead to alterations in the disposition of globular domain and thereby affect resident functions such as NHEJ and Tel1 activation (Hohl et al., 2011).

Therefore, we examined the repair of a single HO DSB in a strain lacking a homologous template (Moore and Haber, 1996). Survival after short (2 hours) HO-induction led to 41.3% survival in wild-type cells, compared to 0.7% in *rad50*Δ. The *rad50*^{hook} mutants exhibited NHEJ defects, with of 3.2%, 9.2%, and 22.1% viability of *rad50-46, -47*, and *-48* respectively (Figure 3D), compared to 41% in wild type cells. In all *rad50*^{hook} mutants, the frequency of imprecise rejoining was increased (Figure 3D, middle and Figure S4A). Quantitative PCR to measure rejoining of the HO site was consistent with cell survival outcomes; negligible rejoining was evident at 5 hours post HO-induction in *rad50-46* and *rad50*Δ cells (Figure 3D, right panel).

Similar defects were evident upon chronic HO-induction. Although cell survival was close to wild types, DNA sequence analysis of NHEJ junctions revealed that the *rad50-46, -47*, and *-48* repair products predominantly exhibited the *rad50*Δ deletion phenotype (Moore and Haber, 1996), characterized by small insertion (mostly +CA) events (Figure 3E, right panel; NHEJ junctions are listed in Figure S4B).

These data show that NHEJ phenotypes of the *rad50*^{hook} mutants are essentially identical to those imparted by truncation of the coiled coil domain (Hohl et al., 2011), and support the view that hook mutations impair the alignment of DNA ends within the globular domain during DSB repair (Williams et al., 2008), resulting in a increased fractions of imprecise repair events at the concomitant expense of reducing precise NHEJ events.

Hook mutants are defective in checkpoint functions

The Mre11 complex is a DSB sensor that activates the ATM/Tel1 pathway, which in budding yeast governs DNA damage responses (DDR) and telomere maintenance (Stracker and Petrini, 2011; Tsukamoto et al., 2001; Usui et al., 2001). As a result, Mre11 complex deficiency is associated with short telomeres (Ritchie and Petes, 2000). Telomere length was determined by Southern blotting of freshly dissected *(rad50*^{hook}*/RAD50)* spores propagated for 10, 30 and 50 generations (Figure 4A). *rad50-46* telomere length was indistinguishable from *rad50*Δ, but marginally longer in *rad50-47* and *rad50-48.* These data suggested an underlying defect in Tel1 activation.

We have previously shown that Mec1-deficiency is partially suppressed in *sae2*Δ cells in a Tel1 and Mre11 complex dependent manner—the TM pathway, culminating in hyper-phosphorylation of the Rad53 effector kinase (Usui et al., 2001). The TM pathway thus

offers a sensitive means to query the ability of Mre11 complex variants to effect Tel1 activation. In Rad50 proficient cells, in which the TM pathway is operative (Usui et al., 2001), *sae2*Δ suppressed *mec1*Δ MMS sensitivity (Figure 4B) and restored Rad53 phosphorylation (Figure 4C) to essentially wild-type levels. This suppression was absent in *rad50^{hook}* mutants; the MMS sensitivity of *rad50-46 mec1*Δ and *rad50-47 mec1*Δ was indistinguishable from *rad50*Δ *mec1*Δ and *rad50-C1G mec1*Δ, whereas *rad50-48 mec1*Δ was slightly less sensitive but unaltered by *sae2*Δ. Rad53 activation, as inferred from phosphorylation, was absent in all three mutants (Figure 4C). These data demonstrate that the *rad50^{hook}* alleles separate Mre11 complex role in DSB repair from its role in Tel1 activation and provide further evidence of the interdependence of the hook and globular domains of the Mre11 complex.

rad50^{hook} mutations and DSB end processing

Meiosis is a specialized program, in which a DSB created by the topoisomerase II like enzyme, Spo11, induces recombination between homologous chromosomes to establish a physical linkage essential for proper chromosome segregation (Borde and de Massy, 2013). The Mre11 complex is required for Spo11-dependent DSB formation, for removal of Spo11 from the DSB end, and for timely repair of meiotic DSBs (Cherry et al., 2007; Keeney, 2008). Sporulation efficiency and viability were severely impaired in *rad50-46* (1.3%, 4.3%) and *rad50-47* (5.7%, 50.6%), whereas *rad50-48* (63%, 88%) was closer to wild-type (81%, 96.8%) in both respects (Figure 5A).

The sporulation defects in *rad50-46* and *-47* were associated with a failure to process meiotic DSBs (Figure S5), phenocopying *rad50S, mre11-3* and *sae2*Δ which are deficient in removal of Spo11 covalently attached to the DSB end (Alani et al., 1990; Cao et al., 1990; Hunter and Kleckner, 2001; Keeney and Kleckner, 1995; Prinz et al., 1997). As expected, recombination at the *HIS4LEU2* hotspot assessed by Southern blotting (Hunter and Kleckner, 2001; Schwacha and Kleckner, 1997) was essentially undetectable in *rad50-46* and *rad50-47* over a 24 hour time course, phenocopying *dmc1*Δ (the meiotic *rad51* ortholog) and *rad50S* (Figure 5C, quantification on right), both deficient in the initiation of meiotic recombination. Genetic assessment of recombination frequencies was also consistent with the interpretation that *rad50-46* and *rad50-47* are largely deficient in initiation of meiotic recombination (Figure S5B).

The removal of Spo11 from DSB ends is partially dependent on the Mre11 nuclease (Moreau et al., 1999), and the data above raised the possibility that this function was impaired in *rad50^{hook}* mutants. As Mre11 nuclease function also promotes the resolution of topoisomerase I adducts in vegetatively growing cells (Foster et al., 2011; Hartsuiker et al., 2009; Mimitou and Symington, 2010; Morales et al., 2008), we measured CPT sensitivity in *rad50-46, -47*, and *-48* cells to assess the effect of *rad50^{hook}* mutations on Mre11 nuclease function. In contrast to MMS and HU, *rad50-46* was acutely sensitive to CPT, exhibiting at least 100 fold greater sensitivity to 5 μM CTP than either *sae2*Δ or *mre11-3* (Figure 1C and Figure S1).

Consistent with the interpretation that the Rad50 hook domain influences Mre11 nuclease function, DNA end resection of an HO-induced DSB at the *MAT* locus assessed by alkaline

electrophoresis and southern blot analysis in G2-arrested cells (Mantiero et al., 2007) was impaired in *rad50-46* cells (Figure 6A), however not to the extent as observed in *rad50*Δ cells (Ivanov et al., 1994). The DSB end resection delays of *rad50-47* and *rad50-48* were slightly milder than the one of *rad50-46* (data not shown).

The extreme sensitivity of *rad50-46* to CPT and the pronounced effect on DSB resection suggested that the effect of that mutation extended beyond Mre11 nuclease function. This interpretation was confirmed in *rad50-46 sae2*Δ and *rad50-46 mre11-3* double mutants. *sae2*Δ, and to a greater extent *mre11-3* double mutants, essentially phenocopied *rad50*Δ in the response to CPT, MMS or HU (Figure 6B). Consistently, loss of Sae2 also profoundly sensitized *rad50-47* and *rad50-48* cells to MMS and CPT (data not shown). Collectively, these data indicate that the hook domain influences Mre11 complex nuclease function and suggest that in *rad50-46 (*and other *rad50*^{hook} mutants), it may pose an impediment to the Exo1 and Dna2, the resection machinery functioning downstream of Mre11 (Mimitou and Symington, 2009).

Intragenic *rad50-46* suppressors within hook, coiled coil and globular domain

The *rad50*^{hook} mutants described herein impair NHEJ, Tel1 activation, and DSB end processing, all of which appear to be mediated by the globular domain of the Mre11 complex. Mechanistic insight regarding this issue came from the identification of intragenic suppressors of the *rad50-46* phenotype.

Four spontaneous chromosomal suppressors arose in the course of strain propagation. DNA sequencing of the *rad50-46* ORF in the apparent revertants revealed that three of the four were intragenic; two contained a N873I mutation within the coiled coil domain, and one changed the Y688E codon to Y688K, converting *rad50-46* to a mutant alike *rad50-48* (S685R Y688R). The ability of N873I to suppress *rad50-46* supported the idea that alterations in hook structure are transduced via the coiled coil domains, and manifest in the globular domain. Additional suppressors were obtained via random mutagenesis of the *rad50-46* ORF from amino acid G78 to S1075 on a centromeric plasmid transformed into *rad50*Δ cells (see Figure 7A). Plasmids were recovered from MMS resistant colonies, and re-confirmed in a second *rad50*Δ transformation (Figure 7B and Figure S6). Eighteen additional suppressors were obtained, ten of which reverted one or both of the *rad50-46* mutations. Of the eight remaining, five were within the hook domain (I680V/T, K700Q/R, L703F), one within the antiparallel coiled coil domain apposing N873I (N607Y), and two within the globular domain (P168S, S193F) (Figure 7A and Figure S6).

We examined the effect of suppressor mutations on the interaction between Mre11 and Rad50-46 (Figure 7C). The *L703F* allele restored the interaction, consistent with its pronounced effect on MMS resistance (Figure 7B). Mre11 interaction was also partially improved in I680V, K700Q V285A, N607Y, N873I and S193F, but suppression of MMS survival was not strictly correlated with restoration of Mre11 interaction, as exemplified by K700Q and P168S. That was also true for the partial suppression of the *rad50-46* telomere and meiotic defects (Figure S7).

We considered two mechanistic possibilities for the observed suppression, both of which are based on the premise that changes in secondary structure were the underlying basis of *rad50-46*, *-47*, and *-48* phenotypes. In one scenario, the suppressor mutations would alter the coiled coil secondary structure and thereby normalize the $Rad50^{hook}$ Zn^{2+} coordination and dimerization behavior. In the alternative scenario, manifestation of secondary structure changes distal to the hook domain mutations would be normalized in the suppressors without normalizing Zn^{2+} coordination behavior of the mutant.

To address these hypotheses, peptides (41-mer) spanning the hook domain and the proximal coiled coil region were synthesized. These peptides were large enough to accommodate the *rad50-46* alterations in combination with I680V, K700Q or L703F suppressor mutations (Figure 7D). Changes in secondary structure induced by Zn^{2+} binding were assessed by circular dichroism (CD). CD titrations of the wild-type peptide exhibited characteristic inflections in ellipticity at 203, 211, and 222 nm, indicating preferential formation of the 2:1 peptide : Zn^{2+} complex. The CD spectra for the wild-type recorded at 2:1 and 1:1 peptide : Zn^{2+} ratios indicate substantial conformational changes upon Zn^{2+} binding (Figure 7E). Conformational changes upon Zn^{2+} binding of the Rad50-46 hook peptides were much less pronounced. No significant changes in the shape of CD and UV (LMCT) titration curves were observed in absence or presence of the suppressor mutations (Figure 7E) and the CD spectra at 2:1 and 1:1 peptide:Zn^{2+} ratios were only slightly altered by the suppressor mutations (Figure 7E, top and middle). Also, zinc binding was largely unaltered in absence or presence of suppressor mutations (Figure 7E, bottom). Consistently, in yeast 2-hybrid analysis assessing hook homodimerization, the I680V, K700Q or L703F suppressors failed to significantly alleviate reporter activation of *rad50-46* hook peptides (Figure S2D).

These data suggest that suppression of *rad50-46* was more likely the effect of secondary structural changes in the coiled coils distal to the hook domain than an effect on Zn^{2+} binding characteristics of the *rad50-46* hook. This interpretation is also consistent with the observation that four of the eight suppressors fell within the coiled coil and globular domains.

If *rad50-46* suppression reflected compensation for structural perturbations distal to the hook domain, we reasoned that mutations, which suppress *rad50-46*, would modify other mutations that impart similar alterations. Thus the ability of the N837I *rad50-46* suppressor to suppress *rad50-47* was assessed. The same mutation was also introduced in the *rad50-C1G* cysteine mutant and $rad50^{sc}$ and $rad50^{sc+h}$, in which the coiled coil domain is truncated without or with the hook domain present respectively (Hohl et al., 2011). The *N873I* mutation suppressed *rad50-47* and $rad50^{sc+h}$ (Figure 7F), indicating that suppression is not specific to *rad50-46*. In contrast, *N873I* failed to suppress *rad50-C1G* and $rad50^{sc}$, indicating that suppression requires a functional hook domain.

In summary, the behavior of $rad50^{hook}$ mutants suggests that the geometry of the hook and coiled coil domain strongly influences the stability and the structural disposition of Mre11 complex globular domain. These outcomes would account for the myriad defects in functions specified by domains within the globular domain.

DISCUSSION

The Rad50 hook domain is an invariant feature of the Mre11 complex, present in all Rad50 orthologs identified. Deletion of the Rad50 hook domain phenocopies complete deficiency in any member of the complex (Hopfner et al., 2002; Stracker and Petrini, 2011). This observation does not address the possibility that only a subset of Mre11 complex functions are directly influenced by the hook domain, and others indirectly. It does appear that hook-mediated dimerization is critical, as replacement with an artificial dimerization cassette is sufficient to restore most Mre11 complex function (Lee et al., 2013; Wiltzius et al., 2005). We reasoned that hypomorphic mutations affecting the Rad50 hook domain that leave it otherwise intact would provide a means to reveal which functions are acutely dependent on the hook domain. In this study, we examined three *rad50*^{hook} alleles (*rad50-46*, *-47*, and *-48*) affecting residues flanking the invariant cysteines of the *S. cerevisiae* Rad50 hook domain.

Biochemical, biophysical and genetic analyses indicate that hook-mediated dimerization is not abolished, but was compromised by these mutations. Consistent with the view that dimerization occurred in *rad50*^{hook} mutants, double strand break repair by SCR was largely intact. This was illustrated by the response of the mutants to clastogens, wherein *rad50-46* was most sensitive, but markedly more resistant than the *rad50*Δ or *rad50-C1G* mutants (Figure 1C). Plasmid based physical analyses of SCR over a 9 hour time course also supported the interpretation that SCR was relatively normal in the *rad50*^{hook} mutants, although occurring with reduced kinetics in *rad50-46* and *rad50-47* (Figure 3B).

We have proposed previously that SCR requires bridging of sister chromatids via Rad50 hook domain dimerization (Hohl et al., 2011; Hopfner et al., 2002; Wiltzius et al., 2005). That model must be reconsidered in light of the data presented here, as it is contradicted by the fact that impaired hook-dependent dimerization in *rad50*^{hook} mutants had only a modest impact on SCR. We consider two possibilities to account for this apparent discrepancy. Atomic force and electron microscopy show that dimerization via the hook domain can occur between Rad50 molecules within a dimeric assembly (*i.e.*, intra-complex), or between Rad50 molecules in separate dimeric assemblies (*i.e.*, inter-complex) (Figure 1B) (Lee et al., 2013; Moreno-Herrero et al., 2005; Williams and Tainer, 2005). Bridging of sister chromatids would presumably require inter-complex dimerization. Hence, our data may suggest that the *rad50*^{hook} alleles impair intra-complex dimerization but have a relatively small impact on inter-complex interactions (Figure 1B). A second possibility is based on the observation that the Mre11 complex is abundantly and avidly associated with chromatin during S phase (Mirzoeva and Petrini, 2003). In this scenario, the increased valency of hook domain interfaces may compensate for the fact that the stability of each individual interface is weakened. Further compensation in this regard may come from cohesin, which is recruited to stalled replication forks and sites of DNA damage (Tittel-Elmer et al., 2012; Unal et al., 2004). It may be that inter-complex interactions, though labile in the mutants, are sufficiently long-lived to foster cohesin recruitment, compensating for reduction in hook-mediated bridging. In this view, the importance of SCR bridging via intercomplex interactions would be minimal.

Apart from SCR, the *rad50*^{hook} mutations affected a broad range of Mre11 complex functions. The non-SCR functions affected are primarily attributed to protein domains lying within the globular domain. Based on the fact that the hook domain is so far distal to the globular domain, we propose that these outcomes reflect the potential of the hook domain to exert long range influence on Mre11 complex secondary structure, including the stability and disposition of the globular domain. It is important to consider, unlike the hook point mutations described here, that complete loss of the hook domain, either by proteolytic cleavage or by genetic deletion does not disrupt Mre11-Rad50 interaction (Hohl et al., 2011; Wiltzius et al., 2005). Hence, it is the structure of the hook, rather than its presence or absence that leads to transduction of structural information between the hook and globular domains via the coiled coils.

This potential was first suggested by the observation that mutation of the invariant cysteines disrupted the interaction between Mre11 and Rad50 (Hopfner et al., 2002), and further indicated by the impact of the *rad50*^{hook} alleles on the Rad50-Mre11 interaction shown here (Figure 3A). Such an influence was also suggested by the observation that SCR was largely proficient in the *rad50*$^{sc+h}$ mutant, which harbors a truncation of the coiled coil domain abutting the hook domain, also conferred defects in NHEJ, telomere maintenance, and meiotic DSB formation (Hohl et al., 2011). The fact that *rad50*^{hook} and the *rad50*$^{sc+h}$ mutations are suppressed by mutations within the coiled coil and globular domains also strongly supports the idea that changes in secondary structure underlie *rad50-46* (as well as *rad50-47* and *rad50-48*) phenotypes, and that the suppressors compensated in some way for those aberrant secondary structures. Collectively, the data suggest that *rad50*^{hook} alleles are not simply hypomorphic. Rather, they provide separations of function that reveal the long range influences of the hook domain.

Tel1 activation defects are common to all *rad50*^{hook} (Figure 4) and *rad50*^{coils} mutations (Hohl et al., 2011). Recent biochemical analyses of the human Mre11 complex provide a potential mechanistic basis for this observation (Lee et al., 2013). The data suggest that the primary functional significance of intra-complex hook-mediated dimerization, which is compromised in the *rad50*^{hook} alleles, is to promote assembly of Rad50 and Mre11 dimers within the globular domain, facilitating ATP binding and hydrolysis critical for ATM (and likely Tel1) activation (Lee et al., 2013).

In this regard, *rad50-48* was unique. This mutant was essentially wild-type in all respects but defective in Tel1 activation. Nevertheless, it was indistinguishable from *rad50-46* and *-47* mutant peptides with respect to impaired dimerization inferred from LMCT (Figure 2B) and yeast 2-hybrid analysis (Figure S2C). Hence, in this instance, impaired dimerization was circumscribed, and linked only to defective Tel1 activation, consistent with the view that intra-complex dimerization is required for this Mre11 complex function (Lee et al., 2013). The broader phenotypic effects of *rad50-46* and *-47* likely reflect that those mutations impart more extensive secondary structural alterations. Supporting this view, the severity of *rad50*^{hook} phenotypes is correlated with the extent to which interaction between Rad50 and Mre11 is compromised; most in *rad50-46*, least in *rad50-48* (Figure 3A).

The effect of the hook domain on Tel1 activation is conserved. We established *rad50-46* and *rad50-47* mouse mutants, and found that ATM activation was abolished in $Rad50^{46/\Delta}$ cells (Roset et al., 2014). Notably, neither homozygote was viable at either the cellular or organismal level, but both alleles exerted a pronounced dominant negative effect. $Rad50^{46/+}$ mice were prone to liver cancer, and exhibited myriad abnormalities, whereas $Rad50^{47/+}$ mice were inviable, indicating that the $Rad50^{47}$ allele had a dominant lethal effect. These data indicate that the influence of the hook domain interface is conserved and can be exerted across the interface to alter the function of wild-type interacting partners (Roset et al., 2014).

Collectively these data demonstrate that the dimerization state of the Rad50 hook domain exerts diverse influences on Mre11 complex function. The influence appears to be manifest, at least in part as structural modulation of the globular domain. On this basis, we propose that the transitions between the open and closed forms of the Mre11 complex described for the globular domain (Lim et al., 2011; Williams et al., 2011; Wyman et al., 2011) are interdependent with transitions in the mode of hook-mediated dimerization. Together, these large scale structural transitions of the complex likely hold the key(s) to the regulation of its diverse functions in the DDR.

EXPERIMENTAL PROCEDURES

Yeast strains and manipulations

Yeast strains used in this study were in the W303 *(RAD5)*, DBY745 or SK1 background and are listed in Table S1. Details of yeast manipulations, plasmid and yeast strain constructions are specified in the Supplemental Experimental Procedures or are available upon request. P values were calculated using the two tailed Wilcoxon rank sum test.

Fluorescence anisotropy, UV titration and CD spectroscopy

Biophysical experiments were performed as previously described (Kochanczyk et al., 2013) and further information are provided in the Supplemental Experimental Procedures.

Other Yeast methods

DNA damage survival assays, yeast extract preparations, co-immunoprecipitation (CoIP), sister chromatid recombination, heteroallelic recombination, nonhomologous end-joining, telomere length and HO-DSB end resection were assessed essentially as previously described (Hohl et al., 2011) with minor modifications specified in the Supplemental Experimental Procedures section.

Supplementary Material

Refer to Web version on PubMed Central for supplementary material.

Acknowledgments

This article is dedicated to the memory of Marlis Hohl.

We are grateful to Jim Haber (Brandeis University), Lorraine Symington (Columbia University), Scott Keeney (Memorial Sloan Kettering Cancer Center) for yeast strains, reagents and technical support. We thank current and

former members of the Petrini laboratory, Tom Kelly and Neil Hunter for critical reading of the manuscript and insightful comments. This work was supported by GM56888 (J.H.J.P.), PBZH33-112756 and PA0033-117484 from the Swiss National Science Foundation and the Eugen and Elisabeth Schellenberg Foundation (M.H.), BFU2010-16372 and Consolider CSD2007-0015 grants from the Spanish Ministry of Economy and Competitiveness (A.A.), 2012/07/E/NZ1/01894 from National Science Centre and FG1/2010, F1/2010/P/2013 from the Foundation for Polish Science (A.K.) and DI2011 031341 from Polish Ministry of Science and Higher Education (T.K.).

References

Al-Ahmadie H, Iyer G, Hohl M, Asthana S, Inagaki A, Schultz N, Hanrahan AJ, Scott SN, Brannon AR, McDermott GC, et al. Synthetic lethality in ATM-deficient RAD50-mutant tumors underlie outlier response to cancer therapy. Cancer discovery. 2014

Alani E, Padmore R, Kleckner N. Analysis of wild-type and rad50 mutants of yeast suggests an intimate relationship between meiotic chromosome synapsis and recombination. Cell. 1990; 61:419–436. [PubMed: 2185891]

Borde V, de Massy B. Programmed induction of DNA double strand breaks during meiosis: setting up communication between DNA and the chromosome structure. Current opinion in genetics & development. 2013; 23:147–155. [PubMed: 23313097]

Bressan DA, Baxter BK, Petrini JH. The Mre11-Rad50-Xrs2 protein complex facilitates homologous recombination-based double-strand break repair in Saccharomyces cerevisiae. Molecular and cellular biology. 1999; 19:7681–7687. [PubMed: 10523656]

Cao L, Alani E, Kleckner N. A pathway for generation and processing of double-strand breaks during meiotic recombination in S. cerevisiae. Cell. 1990; 61:1089–1101. issn: 0092-8674. [PubMed: 2190690]

Cherry SM, Adelman CA, Theunissen JW, Hassold TJ, Hunt PA, Petrini JH. The Mre11 complex influences DNA repair, synapsis, and crossing over in murine meiosis. Curr Biol. 2007; 17:373–378. [PubMed: 17291760]

Cortes-Ledesma F, Aguilera A. Double-strand breaks arising by replication through a nick are repaired by cohesin-dependent sister-chromatid exchange. EMBO reports. 2006; 7:919–926. [PubMed: 16888651]

de Jager M, Trujillo KM, Sung P, Hopfner KP, Carney JP, Tainer JA, Connelly JC, Leach DR, Kanaar R, Wyman C. Differential arrangements of conserved building blocks among homologs of the Rad50/Mre11 DNA repair protein complex. Journal of molecular biology. 2004; 339:937–949. [PubMed: 15165861]

Deshpande RA, Williams GJ, Limbo O, Williams RS, Kuhnlein J, Lee JH, Classen S, Guenther G, Russell P, Tainer JA, et al. ATP-driven Rad50 conformations regulate DNA tethering, end resection, and ATM checkpoint signaling. The EMBO journal. 2014; 33:482–500. [PubMed: 24493214]

Duursma AM, Driscoll R, Elias JE, Cimprich KA. A role for the MRN complex in ATR activation via TOPBP1 recruitment. Molecular cell. 2013; 50:116–122. [PubMed: 23582259]

Foster SS, Balestrini A, Petrini JH. Functional interplay of the Mre11 nuclease and Ku in the response to replication-associated DNA damage. Molecular and cellular biology. 2011; 31:4379–4389. [PubMed: 21876003]

González-Barrera S, Cortés-Ledesma F, Wellinger RE, Aguilera A. Equal Sister Chromatid Exchange Is a Major Mechanism of Double-Strand Break Repair in Yeast. Molecular cell. 2003; 11:1661–1671. [PubMed: 12820977]

Hamman BD, Oleinikov AV, Jokhadze GG, Traut RR, Jameson DM. Dimer/monomer equilibrium and domain separations of Escherichia coli ribosomal protein L7/L12. Biochemistry. 1996; 35:16680–16686. [PubMed: 8988004]

Hartsuiker E, Neale MJ, Carr AM. Distinct requirements for the Rad32(Mre11) nuclease and Ctp1(CtIP) in the removal of covalently bound topoisomerase I and II from DNA. Molecular cell. 2009; 33:117–123. [PubMed: 19150433]

Hohl M, Kwon Y, Galvan SM, Xue X, Tous C, Aguilera A, Sung P, Petrini JH. The Rad50 coiled-coil domain is indispensable for Mre11 complex functions. Nature structural & molecular biology. 2011; 18:1124–1131.

Hopfner KP. ATP puts the brake on DNA double-strand break repair: A new study shows that ATP switches the Mre11-Rad50-Nbs1 repair factor between signaling and processing of DNA ends. BioEssays : news and reviews in molecular, cellular and developmental biology. 2014; 36:1170–1178.

Hopfner KP, Craig L, Moncalian G, Zinkel RA, Usui T, Owen BA, Karcher A, Henderson B, Bodmer JL, McMurray CT, et al. The Rad50 zinc-hook is a structure joining Mre11 complexes in DNA recombination and repair. Nature. 2002; 418:562–566. [PubMed: 12152085]

Huang KN, Symington LS. Mutation of the gene encoding protein kinase C 1 stimulates mitotic recombination in Saccharomyces cerevisiae. Molecular and cellular biology. 1994; 14:6039–6045. [PubMed: 8065337]

Hunter N, Kleckner N. The single-end invasion: an asymmetric intermediate at the double-strand break to double-holliday junction transition of meiotic recombination. Cell. 2001; 106:59–70. [PubMed: 11461702]

Ivanov EL, Sugawara N, White CI, Fabre F, Haber JE. Mutations in XRS2 and RAD50 delay but do not prevent mating-type switching in Saccharomyces cerevisiae. Mol Cell Biol. 1994; 14:3414–3425. [PubMed: 8164689]

Keeney S. Spo11 and the Formation of DNA Double-Strand Breaks in Meiosis. Genome dynamics and stability. 2008; 2:81–123. [PubMed: 21927624]

Keeney S, Kleckner N. Covalent protein-DNA complexes at the 5′ strand termini of meiosis-specific double-strand breaks in yeast. Proc Natl Acad Sci USA. 1995; 92:11274–11278. [PubMed: 7479978]

Kochanczyk T, Jakimowicz P, Krezel A. Femtomolar Zn(II) affinity of minimal zinc hook peptides–a promising small tag for protein engineering. Chemical communications. 2013; 49:1312–1314. [PubMed: 23303248]

Lammens K, Bemeleit DJ, Mockel C, Clausing E, Schele A, Hartung S, Schiller CB, Lucas M, Angermuller C, Soding J, et al. The Mre11:Rad50 structure shows an ATP-dependent molecular clamp in DNA double-strand break repair. Cell. 2011; 145:54–66. [PubMed: 21458667]

Lee JH, Mand MR, Deshpande RA, Kinoshita E, Yang SH, Wyman C, Paull TT. Ataxia telangiectasia-mutated (ATM) kinase activity is regulated by ATP-driven conformational changes in the Mre11/Rad50/Nbs1 (MRN) complex. The Journal of biological chemistry. 2013; 288:12840–12851. [PubMed: 23525106]

Lim HS, Kim JS, Park YB, Gwon GH, Cho Y. Crystal structure of the Mre11-Rad50-ATPgammaS complex: understanding the interplay between Mre11 and Rad50. Genes & development. 2011; 25:1091–1104. [PubMed: 21511873]

Mantiero D, Clerici M, Lucchini G, Longhese MP. Dual role for Saccharomyces cerevisiae Tel1 in the checkpoint response to double-strand breaks. EMBO reports. 2007; 8:380–387. [PubMed: 17347674]

Mimitou EP, Symington LS. DNA end resection: many nucleases make light work. DNA repair. 2009; 8:983–995. [PubMed: 19473888]

Mimitou EP, Symington LS. Ku prevents Exo1 and Sgs1-dependent resection of DNA ends in the absence of a functional MRX complex or Sae2. The EMBO journal. 2010; 29:3358–3369. [PubMed: 20729809]

Mirzoeva OK, Petrini JH. DNA replication-dependent nuclear dynamics of the Mre11 complex. Mol Cancer Res. 2003; 1:207–218. [PubMed: 12556560]

Moore JK, Haber JE. Cell cycle and genetic requirements of two pathways of nonhomologous end-joining repair of double-strand breaks in Saccharomyces cerevisiae. Mol Cell Biol. 1996; 16:2164–2173. [PubMed: 8628283]

Morales M, Liu Y, Laiakis EC, Morgan WF, Nimer SD, Petrini JH. DNA damage signaling in hematopoietic cells: a role for Mre11 complex repair of topoisomerase lesions. Cancer Res. 2008; 68:2186–2193. [PubMed: 18381424]

Moreau S, Ferguson JR, Symington LS. The nuclease activity of Mre11 is required for meiosis but not for mating type switching, end joining, or telomere maintenance. Molecular and cellular biology. 1999; 19:556–566. [PubMed: 9858579]

Moreno-Herrero F, de Jager M, Dekker NH, Kanaar R, Wyman C, Dekker C. Mesoscale conformational changes in the DNA-repair complex Rad50/Mre11/Nbs1 upon binding DNA. Nature. 2005; 437:440–443. [PubMed: 16163361]

Prinz S, Amon A, Klein F. Isolation of COM1, a new gene required to complete meiotic double-strand break-induced recombination in Saccharomyces cerevisiae. Genetics. 1997; 146:781–795. [PubMed: 9215887]

Ritchie KB, Petes TD. The Mre11p/Rad50p/Xrs2p complex and the Tel1p function in a single pathway for telomere maintenance in yeast. Genetics. 2000; 155:475–479. [PubMed: 10790418]

Rojowska A, Lammens K, Seifert FU, Direnberger C, Feldmann H, Hopfner KP. Structure of the Rad50 DNA double-strand break repair protein in complex with DNA. The EMBO journal. 2014

Roset R, Inagaki A, Hohl M, Brenet F, Lafrance-Vanasse J, Lange J, Scandura JM, Tainer JA, Keeney S, Petrini JH. The Rad50 hook domain regulates DNA damage signaling and tumorigenesis. Genes & development. 2014; 28:451–462. [PubMed: 24532689]

Schwacha A, Kleckner N. Interhomolog bias during meiotic recombination: meiotic functions promote a highly differentiated interhomolog-only pathway. Cell. 1997; 90:1123–1135. [PubMed: 9323140]

Shiotani B, Nguyen HD, Hakansson P, Marechal A, Tse A, Tahara H, Zou L. Two distinct modes of ATR activation orchestrated by Rad17 and Nbs1. Cell reports. 2013; 3:1651–1662. [PubMed: 23684611]

Stiff T, Reis C, Alderton GK, Woodbine L, O'Driscoll M, Jeggo PA. Nbs1 is required for ATR-dependent phosphorylation events. The EMBO journal. 2004

Stracker TH, Petrini JH. The MRE11 complex: starting from the ends. Nat Rev Mol Cell Biol. 2011; 12:90–103. [PubMed: 21252998]

Stracker TH, Roig I, Knobel PA, Marjanovic M. The ATM signaling network in development and disease. Frontiers in genetics. 2013; 4:37. [PubMed: 23532176]

Tittel-Elmer M, Lengronne A, Davidson MB, Bacal J, Francois P, Hohl M, Petrini JH, Pasero P, Cobb JA. Cohesin association to replication sites depends on rad50 and promotes fork restart. Molecular cell. 2012; 48:98–108. [PubMed: 22885006]

Tsukamoto Y, Taggart AK, Zakian VA. The role of the Mre11-Rad50-Xrs2 complex in telomerase-mediated lengthening of Saccharomyces cerevisiae telomeres. Curr Biol. 2001; 11:1328–1335. [PubMed: 11553325]

Unal E, Arbel-Eden A, Sattler U, Shroff R, Lichten M, Haber JE, Koshland D. DNA damage response pathway uses histone modification to assemble a double-strand break-specific cohesin domain. Molecular cell. 2004; 16:991–1002. [PubMed: 15610741]

Usui T, Ogawa H, Petrini JH. A DNA damage response pathway controlled by Tel1 and the Mre11 complex. Molecular cell. 2001; 7:1255–1266. [PubMed: 11430828]

van der Linden E, Sanchez H, Kinoshita E, Kanaar R, Wyman C. RAD50 and NBS1 form a stable complex functional in DNA binding and tethering. Nucleic Acids Res. 2009; 37:1580–1588. [PubMed: 19151086]

Williams GJ, Williams RS, Williams JS, Moncalian G, Arvai AS, Limbo O, Guenther G, SilDas S, Hammel M, Russell P, et al. ABC ATPase signature helices in Rad50 link nucleotide state to Mre11 interface for DNA repair. Nature structural & molecular biology. 2011; 18:423–431.

Williams RS, Moncalian G, Williams JS, Yamada Y, Limbo O, Shin DS, Groocock LM, Cahill D, Hitomi C, Guenther G, et al. Mre11 dimers coordinate DNA end bridging and nuclease processing in double-strand-break repair. Cell. 2008; 135:97–109. [PubMed: 18854158]

Williams RS, Tainer JA. A nanomachine for making ends meet: MRN is a flexing scaffold for the repair of DNA double-strand breaks. Molecular cell. 2005; 19:724–726. [PubMed: 16168369]

Wiltzius JJ, Hohl M, Fleming JC, Petrini JH. The Rad50 hook domain is a critical determinant of Mre11 complex functions. Nature structural & molecular biology. 2005; 12:403–407.

Wyman C, Lebbink J, Kanaar R. Mre11-Rad50 complex crystals suggest molecular calisthenics. DNA repair. 2011; 10:1066–1070. [PubMed: 21893433]

- Mre11 nuclease, NHEJ, and Tel1/ATM activation depend on the Rad50 hook domain.
- Rad50 hook domain mutation effects separation of checkpoint and repair functions.
- Mutations in the coiled coil domain suppress defects in the Rad50 hook domain.
- The Rad50 hook domain is partially dispensable for sister chromatid recombination.

Hohl and colleagues show that the Rad50 hook domain, a Zn^{2+} dependent homodimerization interface, influences DNA repair and checkpoint functions of the Mre11 complex. They provide evidence that these influences reflect long range conformational changes in distal regions of the complex controlled by the Rad50 hook domain.

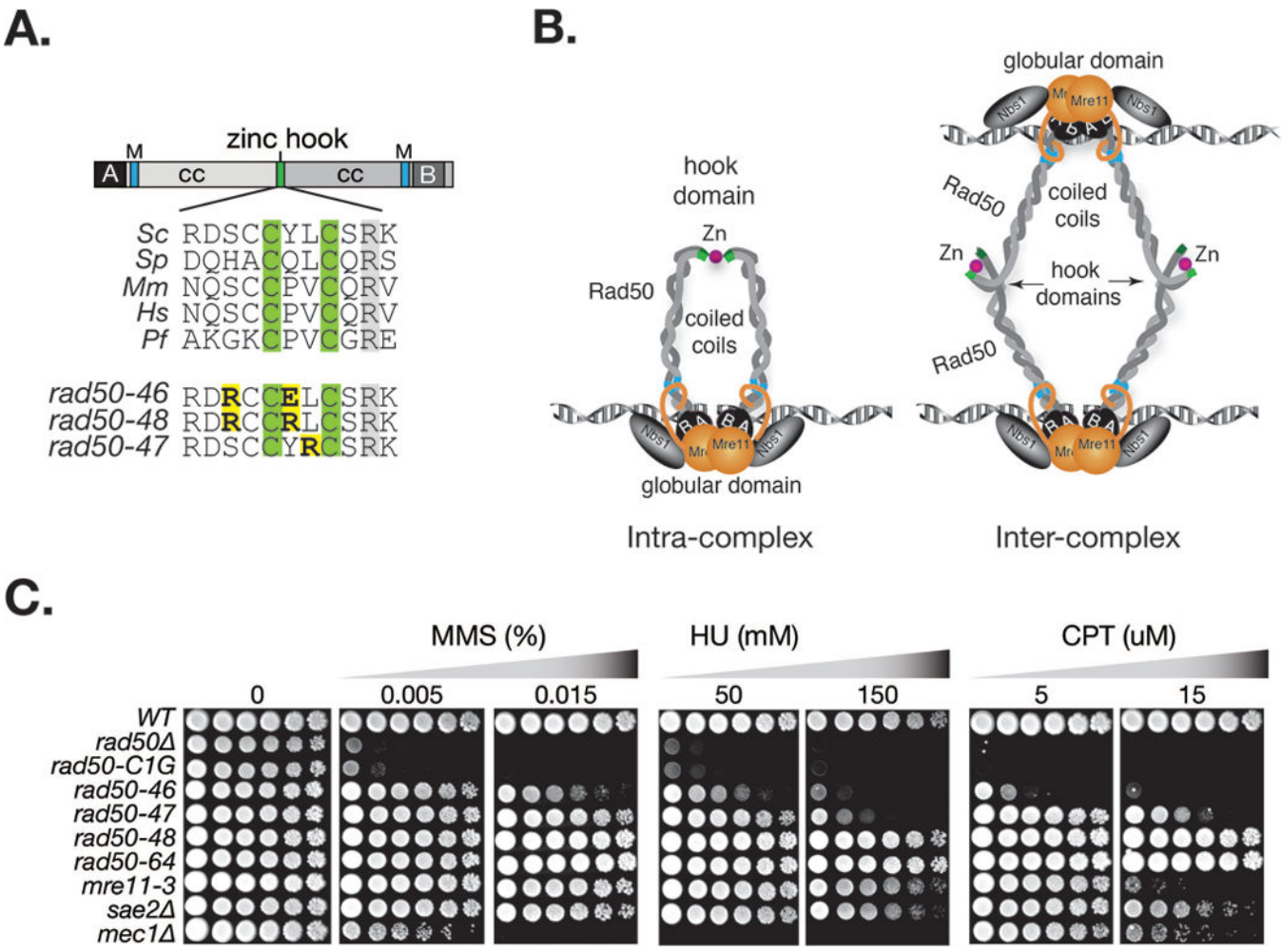

Figure 1. Damage sensitivity of *rad50*^{hook} mutants

A. Rad50 primary domain structure and multiple sequence alignment of the central portion of the Rad50 hook domain. The zinc coordinating hook cysteines are highlighted in green and in yellow the *S. cerevisiae rad50*^{hook} alleles, *rad50-46* (S685R Y688E), *rad50-4 7* (L689R) and *rad50-48* (S685R Y688R). Annotations: coiled coil (cc), Walker A (A), Walker B (B), Mre11 interaction interface (M); *Sc, S. cerevisiae; Sp, S. pombe; Mm, M. musculus, Hs, H. sapiens; Pf, P. furiosus.* **B.** Schematic illustration of Rad50 hook dimerization between Rad50 proteins within a dimeric Mre11 complex assembly (intra-complex) or between Rad50 molecules in separate Mre11 complex dimeric assemblies (inter-complex). **C.** Sensitivities of *rad50*^{hook} mutants to the indicated concentration of MMS, HU and CPT. The *rad50-46* mutational residues were flipped in *rad50-64* (S688E Y688R). Plates were incubated at 30°C. Outcomes at other incubation temperatures are given in Figure S1.

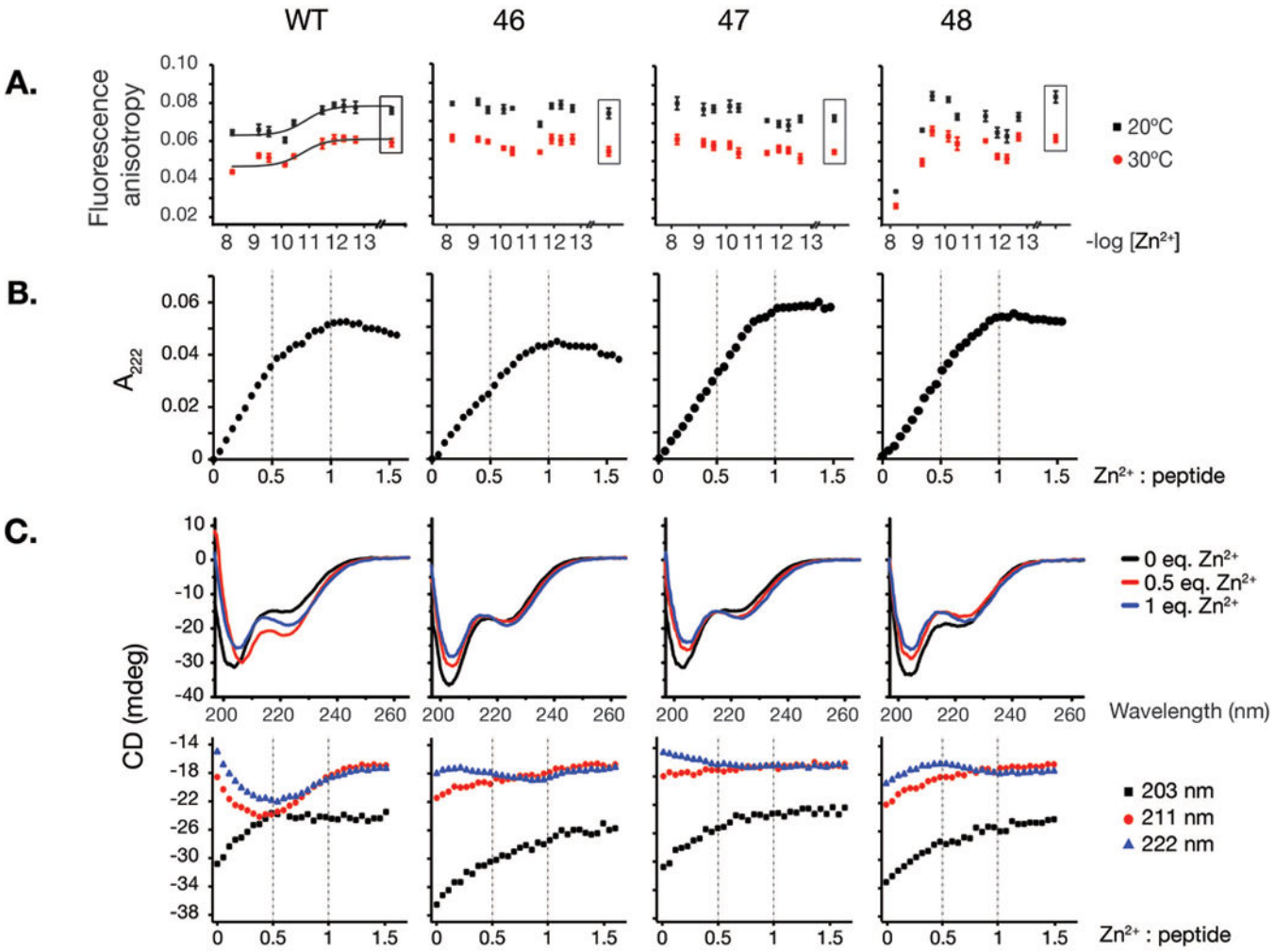

Figure 2. Rad50 hook mutations destabilize hook dimerization

A. Homo-FRET of 5-carboxyfluorescein labeled 68 amino acid long hook peptides. Fluorescence anisotropy values for wild-type and 46, 47, 48 hook mutant peptides incubated in free Zn^{2+}-controlled metal buffers providing various free zinc concentrations ($-\log[Zn^{2+}]$) are plotted. Data points shown in a box reflects buffer without Zn^{2+}, containing chelator only (1 mM EDTA). Data were fitted to Hill's equation with cooperativity coefficient fixed at 1.0. **B.** Titration of 41-mer WT and $Rad50^{hook}$ peptides with Zn^{2+} monitored by spectroscopy at 222 nm. Formation of coordinate bonds is observed as CysS-> Zn LMCT bands that can be monitored in the UV region. **C.** Circular dichroism (CD) spectra of wild-type and Rad50-46 hook mutant 41-mer unlabeled peptides. CD spectra of peptides with 0 (apo-peptide), 2.5 μM (0.5 equivalent of Zn^{2+}) and 5 μM Zn^{2+} (1 eq. of Zn^{2+}) at 203, 211 and 222 nm are given.

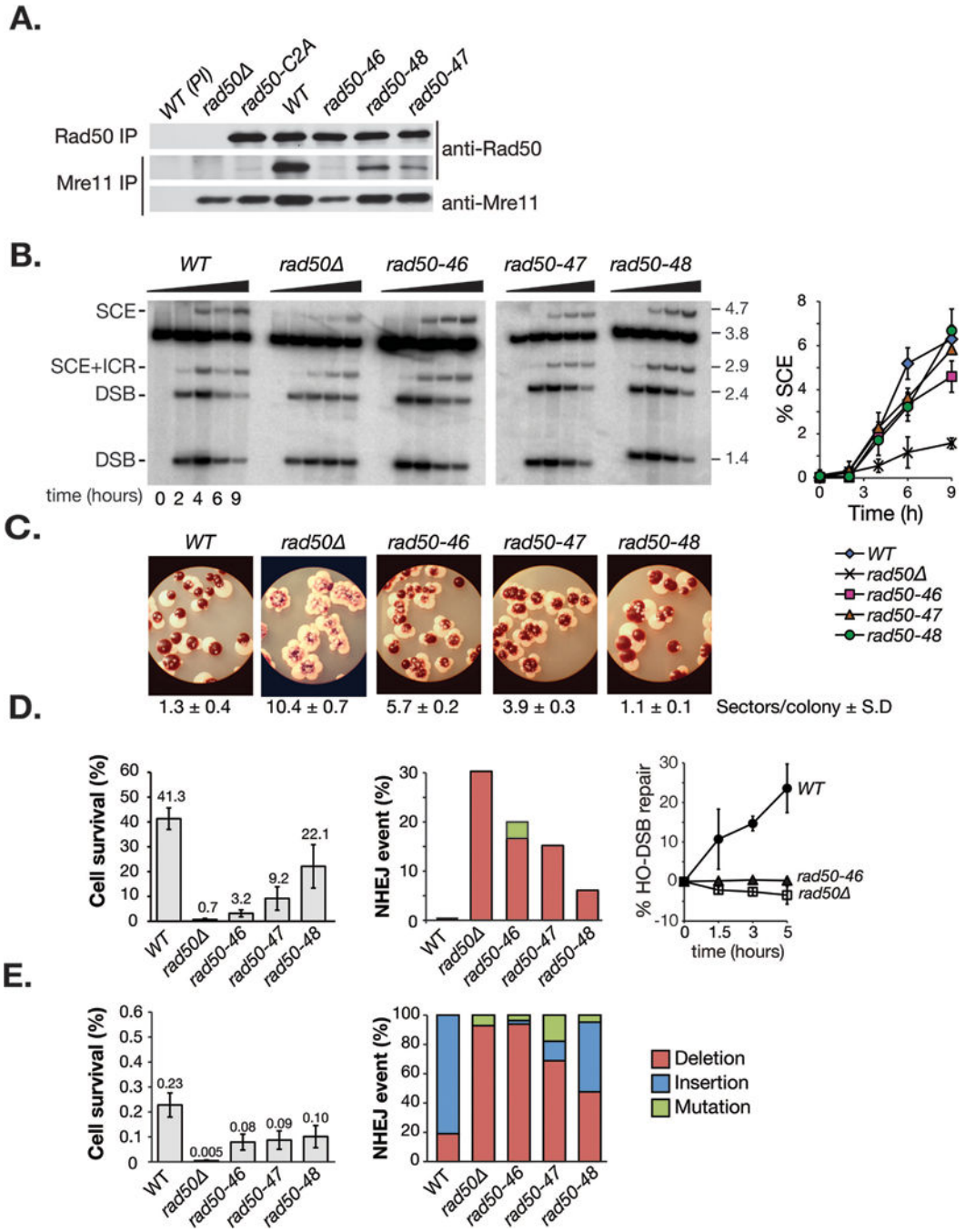

Figure 3. Mre11 complex integrity and DSB repair functions in *rad50*^{hook} mutant cells

A. Mre11 complex integrity in wild-type and *rad50*^{hook} mutants assessed by co-immunoprecipitation and western blot with Rad50 or Mre11 antisera. Pre-immune antibodies (PI) were included as negative controls. **B**. Physical assessment of HO-induced sister chromatid recombination (SCR) as previously described (Hohl et al., 2011). Representative southern blots are shown. Right panel: Quantification of the 4.7 kb band specific for SCR relative to the total DNA. Error bars denote standard deviation from three independent experiments. **C**. Spontaneous *ade2* heteroallelic mitotic recombination in *ade2-*

n/*ade2-l-Scel* heterozygot diploids. White sectors (*ADE2)* within >200 red colonies (*ade2)* were scored. The average number of white sectors per colony for each genotype is given. Standard deviations correspond to 5-7 diploids analyzed. **D**. Cell survival (left panel) and NHEJ repair events (middle panel) after acute (2 hours) HO DSB induction at the *MAT* locus. Error prone NHEJ events detected in *rad50* mutants were categorized as insertion, deletion or point mutation and are given in Figure S4A. Right panel: NHEJ repair kinetics for wild-type, *rad50*Δ and *rad50-46.* Cells were cultivated for 1.5, 3 or 5 hours in glucose medium following HO induction (2 hours) and repair was monitored by quantitative PCR with primers flanking the HO site. Error bars denote standard deviation from at least three independent experiments. **E**. Cell survival upon chronic HO induction. Repair junctions were analyzed and sequences are given in Figure S4B. Error bars denote standard deviation from at least three experiments.

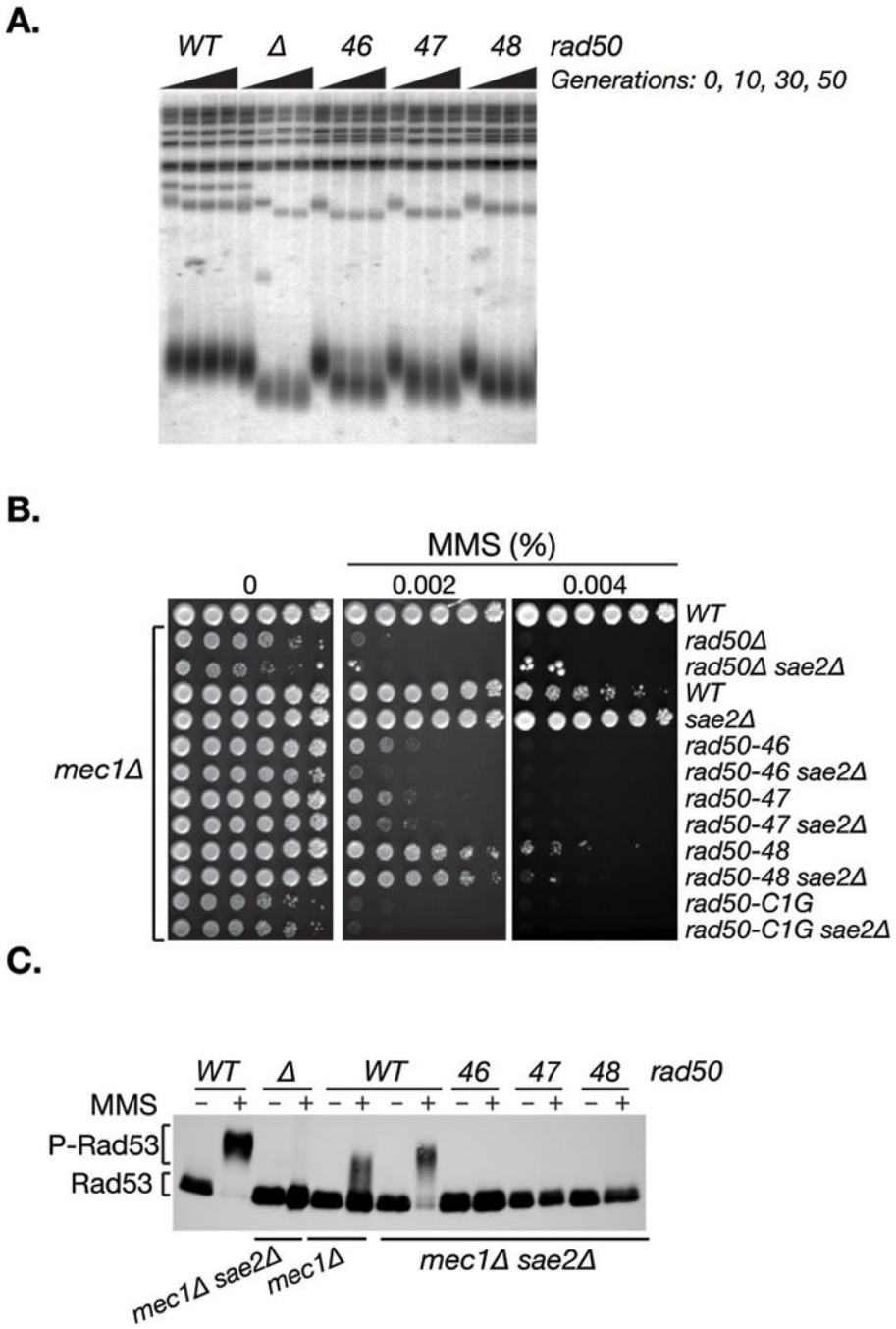

Figure 4. *rad50*^{hook} mutants are defective in telomere maintenance and Tel1 checkpoint signaling

A. Telomere lengths of wild-type and *rad50*^{hook} mutants after 10, 30 and 50 generations of growth at 30°C. Heterozygote diploids (*RAD50/ rad50*^{hook}) were included as 0 generations of growth. **B**. Cell survival of *rad50*^{hook} *mutants* in a Mec1-deficient background. All strains below the wild-type strain (top row) were *mec1*Δ *sml1*Δ. **C.** Tel1-dependent Rad53 phosphorylation in Mec1-deficient cells upon MMS treatment (+) assessed by western blot. The migration levels of the non-phosphorylated (Rad53) and phosphorylated form (P-

Rad53) are indicated. Rad50 genotypes are given above the blot and the Mec1 and Sae2 status (either wild-type or deleted) below.

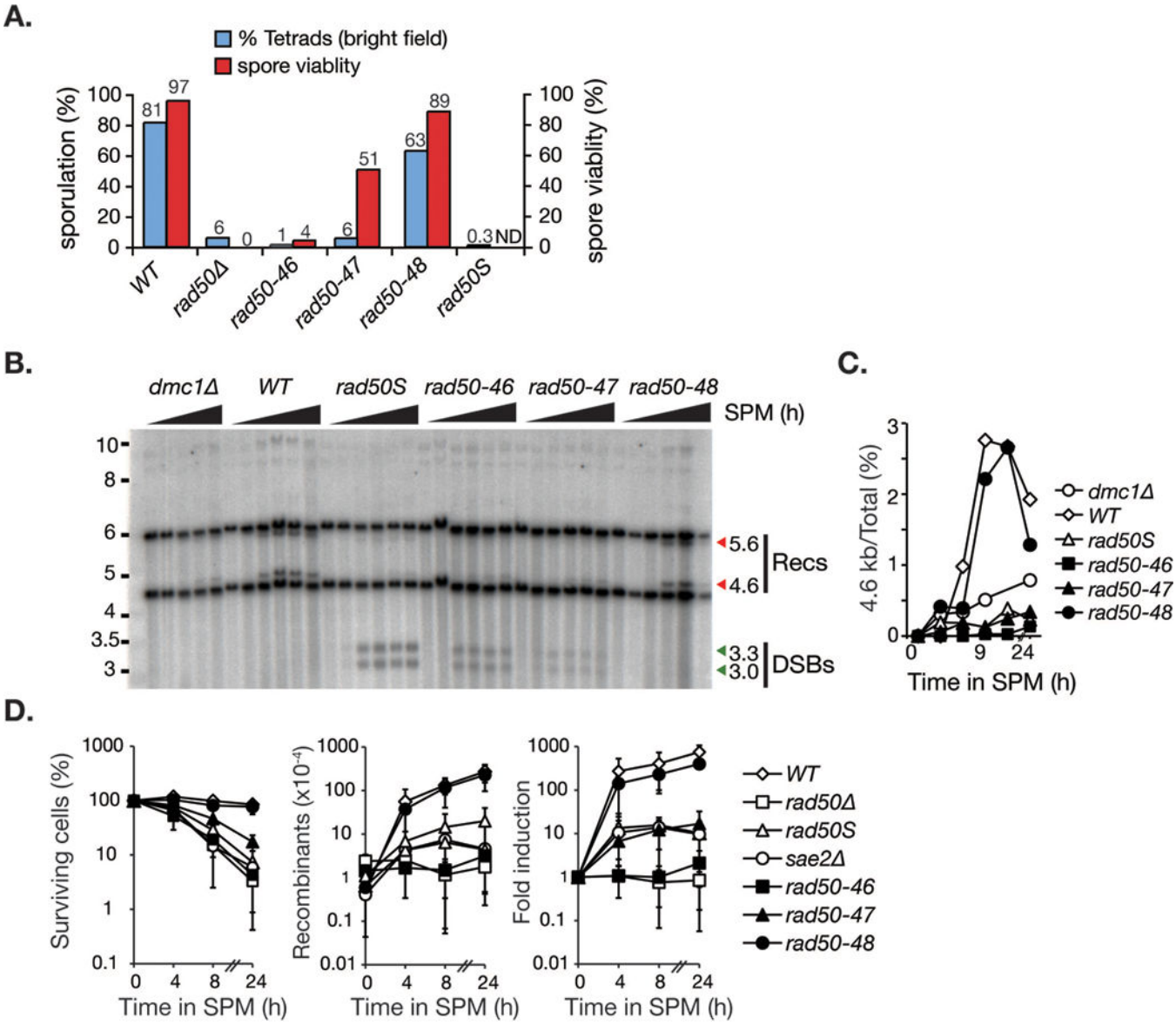

Figure 5. Meiotic DSBs processing is impaired in *rad50-46* and *rad50-47 but* not *rad50-48*

A. Sporulation efficiency (in blue) and spore viability (in red) of the indicated genotypes were assessed in SK1 homozygot diploid cells after 48 hours sporulation. The sporulation efficiency was calculated as the percentage of asci among total number of cells (% tetrads) and graphically illustrated (% sporulation, y-axis on the left). Spore viability was determined by tetrad dissection of at least 30 tetrads (% spore viability, y-axis on the right). Spore viability for *rad50S/S* w*as* not determined (ND). **B.** Meiotic DSB formation and repair by meiotic recombination at the *HIS4-LEU2 hotspot* by southern blot. The migration level of the crossover recombinant fragments (Recs, recombinants; 5.6 kb and 4.6 kb, red arrows) above and below the parental band (Hunter and Kleckner, 2001; Schwacha and Kleckner, 1997) and the unprocessed 3.3 kb and 3.0 kb meiotic double strand break fragments (DSB, green arrows) are denoted. Cells were cultivated in sporulation media (SPM) for 0, 3, 6, 9 and 24 (*dmc1*Δ) or for 0, 3, 6, 9, 12 and 24 hours (*WT*, *rad50S*, *rad50-46*, *rad50-47* and

rad50-48). **C.** Relative signal intensities of the 4.6 kb recombinant fragment versus total counts per lane is shown on the right.

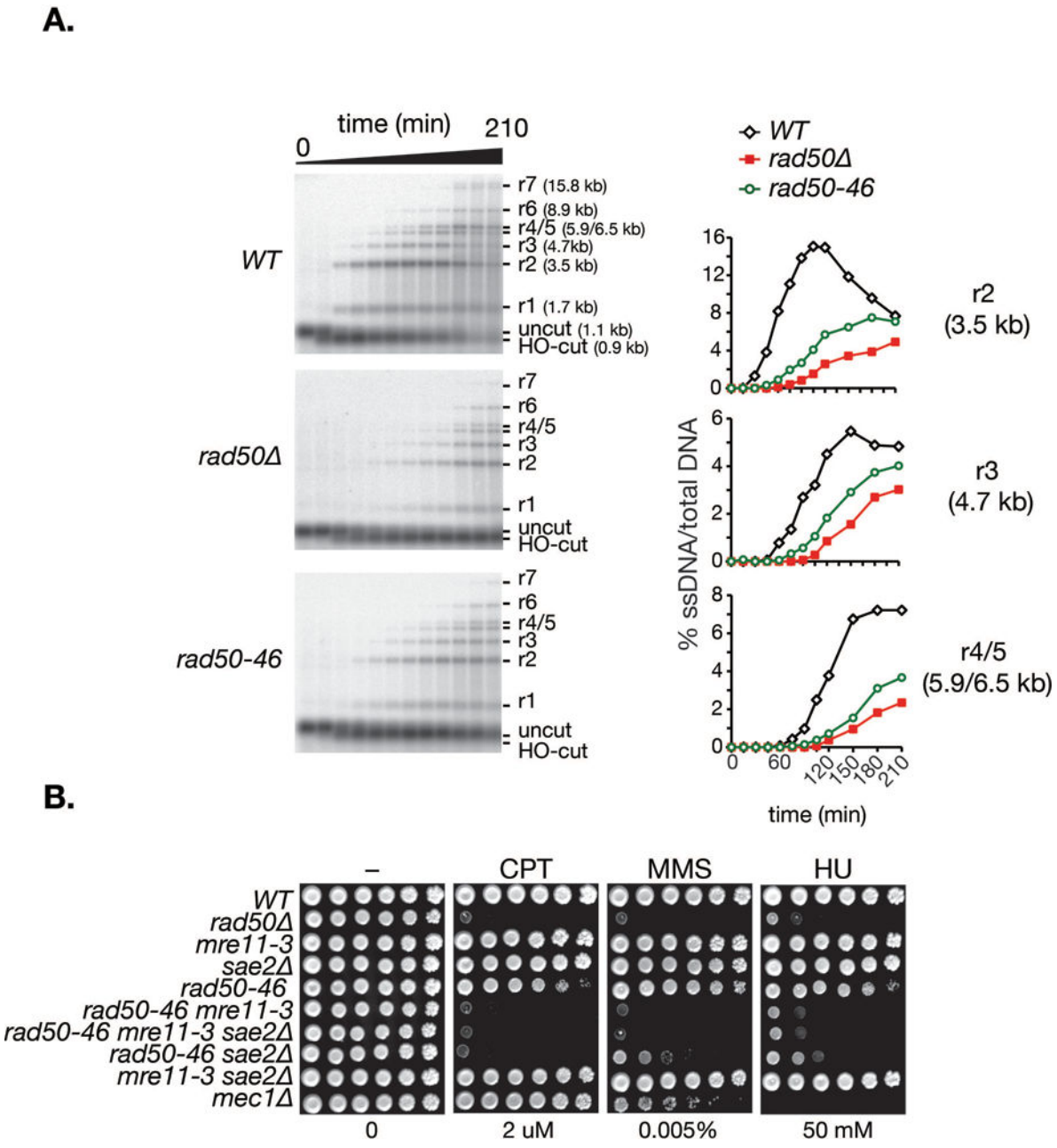

Figure 6. The Mre11 nuclease function is critical for *rad50-46* DSB end resection and damage survival

A. HO-DSB end resection in G2 arrested cells at 30°C in a time course over 210 minutes in wild-type, *rad50-46* and *rad50*Δ cells. 5′-to-3′ end resection products of an HO-DSB are detectable with an ssRNA probe after alkaline gel electrophoresis of *Ssp*I-digested DNA. The migration levels of HO-uncut (1.1 kb), HO-cut (0.9 kb), and resection fragments r1 (1.7 kb), r2 (3.5 kb), r3 (4.7 kb), r4 (5.9 kb), r5 (6.5 kb), r6 (8.9 kb) and r7 (15.8 kb) from the HO-site (HO) are indicated. Right panel: Quantification of the r2, r3 and r4+r5 fragments of the southern blots shown. Similar results were obtained in three experiments. Note that the blots and quantifications for wild-type and *rad50*Δ were previously published elsewhere

(Hohl et al., 2011). **B.** Damage survival of *rad50-46* is dependent on Mre11 nuclease function and Sae2.

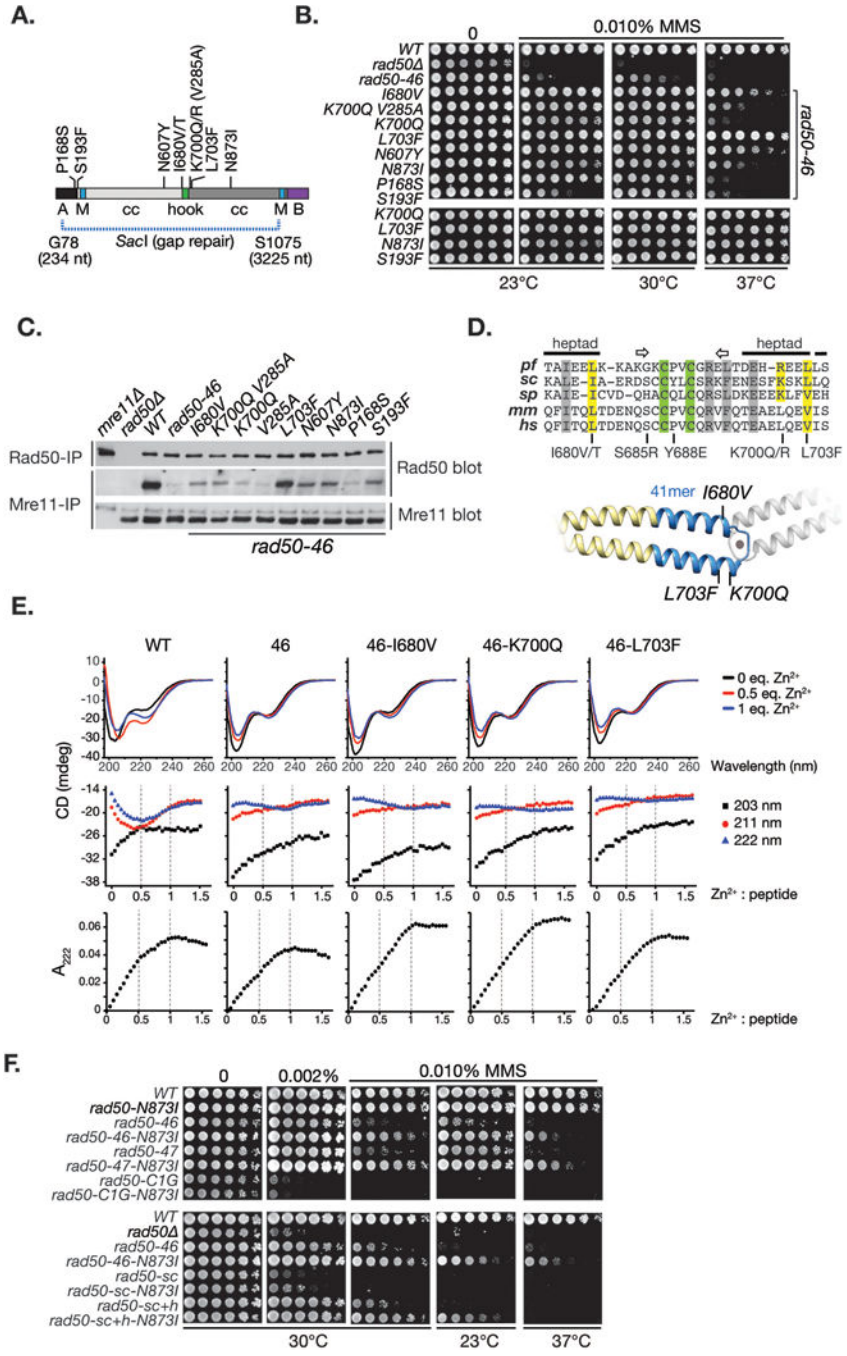

Figure 7. Isolation and phenotypic analysis of *rad50-46* intragenic suppressors

A. Schematic illustration of the genetic screen to isolate intragenic suppressors of *rad50-46* MMS sensitivity at 23°C. *Sac*I digested plasmid *Ycp50-RAD50* (from nucleotide 234-3225, corresponding to amino acid G78 – S1075) was gap repaired in *rad50*Δ cells with a *rad50-46* PCR mutagenized repair template. Cells containing the gap repaired plasmid were plated on selective media containing 0.1% MMS and grown at 23°C. Plasmid were recovered from survivor colonies, re-transformed in *rad50*Δ cells, and suppression was confirmed on MMS plates. Sequenced *rad50-46* suppressors are given. **B.** *rad50-46*

suppressors were re-assessed by spot test on plates with 0.1% MMS, either incubated at 23°C, 30°C or 37°C. Some of the *rad50-46* suppressors were also assessed in context of the wild-type hook domain (bottom 4 strains). **C.** Mre11 complex integrity of *rad50-46* suppressor mutants was assessed by co-immunoprecipitation and western blot with Rad50 or Mre11 antisera as indicated. **D.** Top: Sequence alignment of the central hook domain flanked by one coiled coil heptad repeat. The conserved zinc-cysteines are highlighted in green, *rad50-46* suppressor mutation in yellow and partially conserved residues in grey. Arrows denote a structurally conserved inverted beta-sheet. *pf, P. furiosus; sc, S. cerevisiae; sp, S. pombe; mm, M. musculus; hs, H. sapiens.* Bottom: I-tasser structure prediction of the 41 amino acid (highlighted in blue) hook dimer peptide. The approximate position of the I680V, K700Q and L703F hook suppressor mutations are denoted. **E.** Circular dichroism spectra and UV spectroscopy of wild-type and *rad50-46* hook peptides without and with hook suppressors**. F.** MMS spot test to assess suppression by N873I of other hook and coiled coil mutants. Plates were incubated either at 23°C, 30°C or 37°C.